LINC-NIRVANA

The **L**BT **IN**terferometric **C**amera and
Near-**I**nfra**R**ed / **V**isible **A**daptive
i**N**terferometer for **A**stronomy

A collaborative project of the MPIA Heidelberg, INAF-Arcetri,
Universität zu Köln, and MPIfR Bonn

http://www.mpia.de/LINC

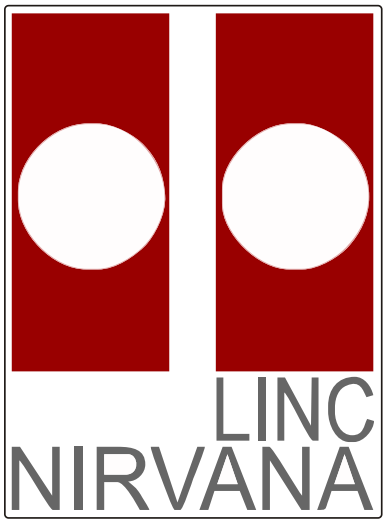

LINC-NIRVANA

—

LINC-NIRVANA in a nutshell. Basic instrument characteristics and performance estimates.

Doc. No.	LN-MPIA-GEN-SCI-001
Short Title	Characteristics and performance
Issue	0.3
Date	08 March 2011

	Name	Date	Signature
Prepared	M. Kürster	08 March 2011	.....
Approved	E. Schinnerer, T. Bertram	dd month, yyyy	.....
Released	M. Kürster	dd month, yyyy	.....

Document Change Record

Issue	Date	Section/Paragraph Affected	Reasons / Remarks
0.1	07 September 2010	All	New document
0.2	24 September 2010	Sect. 5	Comments by T. Bertram implemented
0.3	08 March 2011	All Tables 4, 5, 6, Figs. 4, 7 Sect. 5.14	Comments by E. Schinnerer implemented Updates and corrections New Table 6

Contents

List of Figures

List of Tables

1 Scope

This document provides a collection of the basic characteristics and expected performance of LINC-NIRVANA. An attempt has been made to select information relevant for a science user in order to plan a scientific program. The distinction between LINC-mode and NIRVANA-mode is made throughout the document. As far as applicable a distinction is also made for the expected performance for an "early" and a "late" phase of instrument implementation. See Sect. 4 for the pertinent definitions.

2 Applicable Documents

No.	Title	Number and Issue
AD1	Mid-High Wavefront Sensor Optical and Mechanical Design	LN-INAFA-FDR-AO-001 v1.2
AD2	Ground Layer Wavefront Sensor Opto-mechanics	LN-INAFA-FDR-AO-002 v1.2
AD3	Simulations and estimates of the atmospheric influence on interferometric performance	LN-KOELN-FDR-GEN-001 v1.1
AD4	MCAO simulations	LN-INAFA-FDR-AO-003 v1.2
AD5	Science Filters I. Verification & Acceptance Document	LN-MPIA-VER-OPT-002 v0.1
AD6	FFTS Filters	LN-KOELN-SPEC-OPT-001 v1.0
AD7	IR Beam Combining Optics	LN-MPIA-FDR-OPT-002
AD8	Science detector	LN-MPIA-FDR-ELEC-006 v1.2
AD9	Science detector control pattern	LN-MPIA-FDR-ELEC-007 v1.2
AD10	Error budget	LN-MPIA-FDR-GEN-001 v1.0
AD11	Field rotation	LN-MPIA-TN-SYS-002 v1.1
AD12	Mid High layer Wavefront Sensor Design Report	LN-INAFB-DES-001 v0.1
AD13	Multi-conjugate Adaptive Optics for LINC-NIRVANA	S. Egner, PhD thesis (2006)
AD14	First light AO (FLAO) system for LBT: final integration, acceptance test in Europe and preliminary on-sky commissioning results	S. Esposito et al. (2010), Proc. SPIE Vol. 7736, 773609-1
AD15	Layer Oriented Wavefront sensor for MAD on Sky operations	C. Arcidiacono et al. (2008), Proc. SPIE Vol. 7015, 70155P-2
AD16	MCAO simulations	LN-INAFA-FDR-AO-003 v1.2
AD17	Simulations and estimates of the atmospheric influence on interferometric performance	LN-KOELN-FDR-GEN-001, V1.0
AD18	Design of the Linc-Nirvana Observation Preparation Software (LOPS)	LN-MPIA-DES-ASW-001 v0.1

3 Acronyms and Abbreviations

ADU	Analog-to-digital unit (detector counts)
AO	Adaptive optics
AOS	Adaptive optics scondary (mirror)
DIMM	Differential image motion monitor
EE	Encircled energy
ESO	European Southern Observatory
ETC	Exposure time calculator
FFTS	Fringe and flexure tracking system
FWHM	Full width at half maximum
FoV	Field-of-view
GUI	Graphical user interface
GWS	Ground-layer wavefront sensor
IDL	Interactive data language - scientific data visualization software
LBT	Large Binocular Telescope
LBTO	Large Binocular Telescope Observatory
LDRS	LINC-NIRVANA Data Reduction Software
LOPS	LINC-NIRVANA Observation Preparation Software
MAD	Multi-conjugated adaptive optics demonstrator
MCAO	Multi-conjugated adaptive optics
MHWS	Mid-high-layer wavefront sensor
MIR	Mid-infrared
MPIfR	Max Planck Institute for Radioastronomy
MST	Mean siderial time
MTF	Modulation transfer function
NIR	Near-infrared
PSF	Point spread function
RON	Read-out noise
SNR	Signal-to-noise ratio
TBC	To be confirmed
TBD	To be defined or determined
UT	Universal time
VLT	Very Large Telescope
VLTI	Very Large Telescope Interferometer

4 Definitions

LINC-NIRVANA will combine the radiation from the two 8.4 m primary mirrors of the Large Binocular Telescope (LBT) in so-called "Fizeau" mode. This configuration preserves phase information, and allows true imagery over a wide field of view. LINC-NIRVANA will deliver the sensitivity of a 12 m telescope and the spatial resolution of a 23 m telescope, over a field of $10.5'' \times 10.5''$.

4.1 LINC-mode

In its initial implementation phase the instrument will be offered in the so-called *"LINC-mode"* which provides interferometric near-infrared (NIR) imaging with classical adaptive optics (AO) correction. Here the term "classical" refers to AO correction with a single on-axis natural guide star. Due to the finite isoplanatic patch size, this implies that the AO performance degrades with increasing separation between AO star and scientific target. Generally, this on-axis guide star will also be used as the reference star for the fringe and flexure tracking system (FFTS), and a similar performance degradation occurs with increasing separation from the guide star due to the related finite isopistonic patch size.

It is useful to differentiate between an *"early LINC-mode"* and a *"late LINC-mode"* according to which functionality will become available early-on and which will come only later. In early LINC-mode the FFTS and AO guide star will be very close (within a few arcsec) to the center of the scientific field while in the late mode the guide star can be placed further away (usually though within the iso-pistonic or iso-planatic angle of typically $30''$) thereby accepting the mentioned degradation of performance. Restrictions on the placement of the FFTS guide star are given in Sect. 5.15.1 and Fig. 9.

While the engineering team will continue to commission the instrument toward the more complex NIRVANA-mode (see below), only the LINC-mode will be available for scientific exploitation.

4.2 NIRVANA-mode

The *"NIRVANA-mode"* will finally provide a layer-oriented (two-layer) multi-conjugated adaptive optics (MCAO) correction whose detailed performance will depend not only on the atmospheric conditions (as does classical AO), but strongly also on the detailed asterism of guide stars available, i.e. the number of stars, their spatial distribution, and their magnitudes. A maximum of eight stars will be accessible for the two mid-high-layer wavefront sensors (MHWS), and a maximum of 12 stars for the two ground-layer wavefront sensors (GWS).[1] In both cases these maximum numbers of stars can only be achieved when certain conditions on the geometrical distribution of the stars are met (see Sect. 5.15.3 as well as AD1 and AD2 for details).

4.3 Early and late phases of instrument implementation

Due to the high level of complexity of the LINC-NIRVANA instrument it is anticipated that it will only be possible to reach the final performance goals when experience with the operation of the instrument has built up over time. To guide the scientific user a distinction between performance

[1] There is one sensor of each type on either arm of the instrument so that the light from the two LBT telescopes is corrected individually; see Fig. 1.)

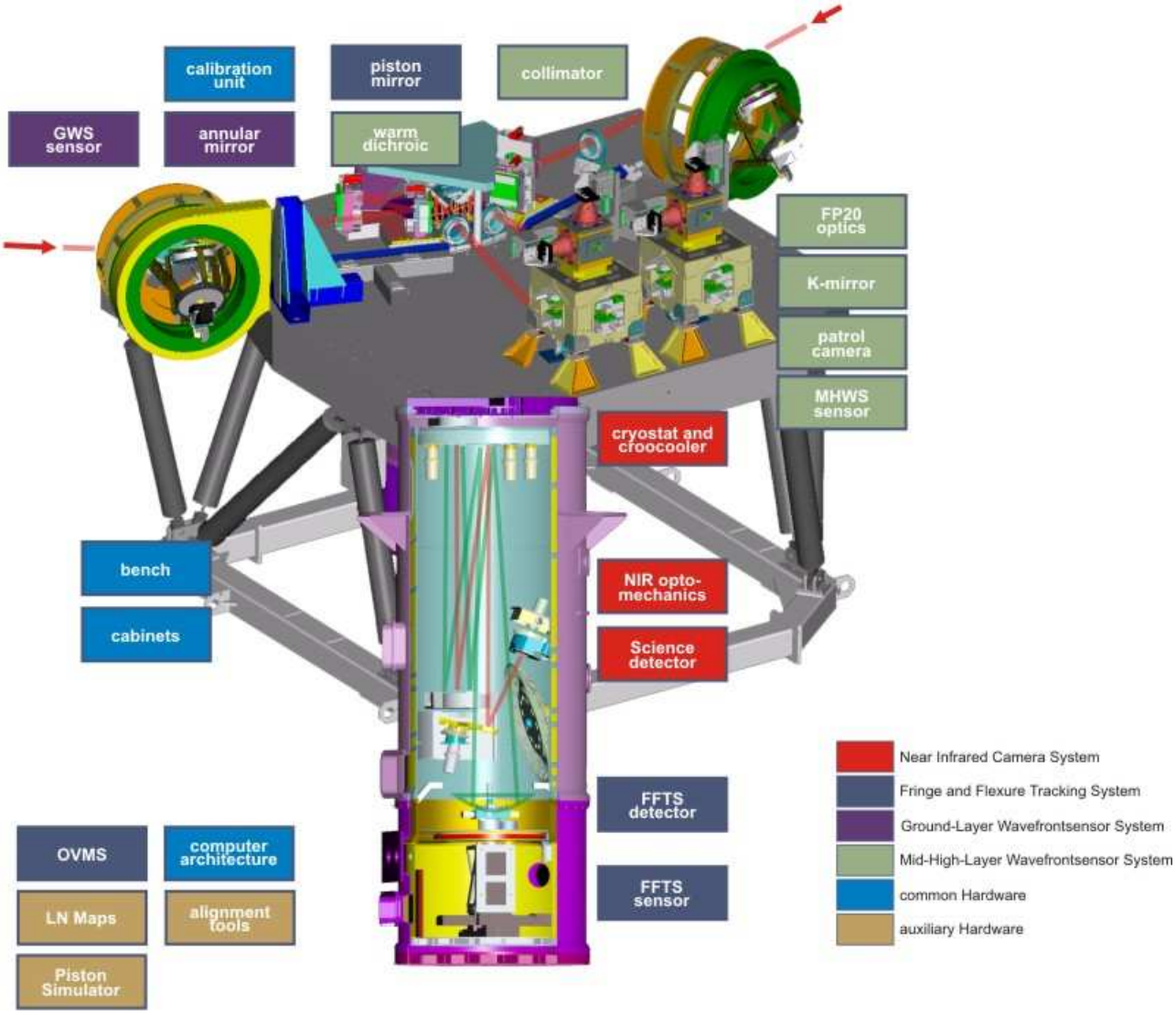

Figure 1: LINC-NIRVANA and its systems and sub-systems.

expectations for an *"early phase"* and a *"late phase"* (in which the overall performance goals are achieved) is in order. Please note that at the time of writing this document most of the performance values are either derived from simulations (see AD3 and AD4) or are pure estimates.

5 Basic properties

5.1 The LINC-NIRVANA instrument

LINC-NIRVANA is an adaptive optics aided near-infrared Fizeau imaging interferometer that will combine the beams from the two telescopes of the Large Binocular Telescope on Mt. Graham in South-Eastern Arizona, USA.

The big advantage of Fizeau interferometry is that it provides wide field, true imagery. In a Fizeau interferometer, the wavefronts interfere in the focal plane, not in the pupil plane as is the case for other interferometer types (such as the Very Large Telescope Interferometer VLTI of the European Southern Observatory ESO). One way to think of a Fizeau interferometer is as a large telescope with a diameter equal to the baseline, but with a mask corresponding to the configuration of component telescopes placed in the entrance pupil. The Fourier transform of this pupil layout is the point spread function (PSF), and all objects within the field display this PSF (see Sect. 5.4 and Fig. 3).

A schematic overview of the systems and sub-systems of the instrument is shown in Fig. 1. For details of the instrument design the reader is referred to the document data base of the project:

https://svn.mpia.de/trac/gulli/ln

https://svn.mpia.de/trac/gulli/ln/wiki/Documents

5.2 LINC-NIRVANA within LBTO

LINC-NIRVANA will be installed at the LBT instrument platform between the rear bent Gregorian foci of the two LBT telescopes. As the last-to-be installed of the first generation of LBT instruments LINC-NIRVANA will be integrated into an operating observatory (LBTO = LBT observatory). Link to LBTO:

http://medusa.as.arizona.edu/lbto/

5.2.1 The LBT

The LBT consists of two 8.4m (diameter) telescopes on a common mount. There are two suitable ways to describe the LBT. Let us first consider only the primary mirrors. On the one hand the LBT can be regarded as a single telescope with a certain distribution of spatial frequencies down to $1/22.8$ m^{-1}, where 22.8m corresponds to its largest optical extent (see Fig. 2). On the other hand, especially when combined with an interferometric instrument such as LINC-NIRVANA, the LBT can be seen as a two-telescope interferometer with a baseline of 14.4m corresponding to the separation of the centers of the two telescopes. Now also the two adaptive secondary mirrors of the LBT must be considered (small blue circles in Fig. 2).[2] With diamters of 90cm each the secondary mirrors are undersized so that the resulting entrance pupil for each telescope has an effective diameter of 8.2m. This results in a minimum spatial frequency of the combined entrance pupil of $\approx 1/22.6$m^{-1}.

LINC-NIRVANA will be installed at the rear bent Greorian foci of both telescopes. In Fig. 2 this location corresponds to the lower part of the area between the two telescopes.

[2] At the time of writing the first adaptive secondary has been successfully installed and tested.

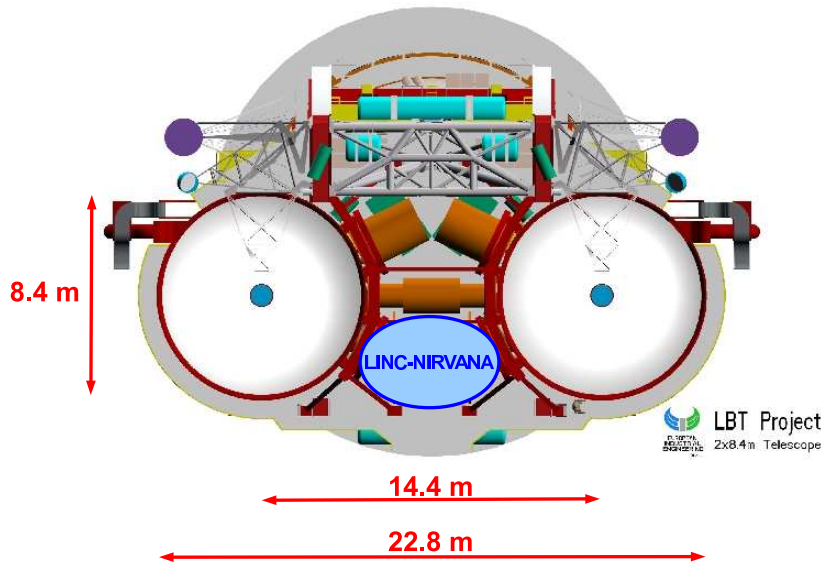

Figure 2: The LBT from above

5.2.2 Mt. Graham

The LBTO is located on Mt. Graham in South-Eastern Arizona, USA. Its geographic coordinates are given by

W 109° 53′ 20.63″, N +32° 42′ 04.71″. The altitude of the observatory is 3221m.

The mean siderial time is given by MST = UT − 7.

5.2.3 The LBT suite of instruments

The following first generation instruments are foreseen for the LBT:

Name	*Type*	*Status*
LBC Blue + Red	Visual wide-field cameras	operational
LUCIFER-1 + 2	NIR imager and multi-object spectrograph	first one operational
ARGOS	Ground layer laser AO system for LUCIFER	under development
MODS-1 + 2	Visual imager and multi-object spepctrograph	first one about to be installed
PEPSI	Visual high-resolution spectrograph	under development
LBTI	MIR interferometer	under development
LINC-NIRVANA	NIR interferometer	under development

5.3 Operating wavelength range and filters

In both the LINC-mode and the NIRVANA-mode the science channel will exploit the wavelength range from $1.0 - 2.45$ μm. Seven filters have already been purchased whose most basic characteristics are summarized in Table 1. More details on these filters such as transmission curves can be found in AD5.

5.3.1 Available filters science channel

Table 1: Basic properties of the defined filters for the science channel

Filter	Central wavelength [μm]	Width @ 50% transmission [μm]
J-short	1.18157	0.11804
J-long	1.30803	0.12022
H	1.64856	0.30068
K	2.21471	0.40828
Pa-β	1.28163	0.01353
Fe II	1.64199	0.01762
Br-γ	2.16902	0.02249

With a total number of 20 filter positions the filter wheel has space for 11 more filters that can still be defined according to the needs of the astronomers. Two of the 20 positions in the filter wheel are reserved for a pupil imager and a blind position, respectively, both of which are needed for technical purposes.

5.3.2 Available filters FFTS channel

The filters planned for use with the FFTS detector can be found in AD6. They are also summarized in Table 2.

Table 2: Basic properties of the FFTS channel filters

Type	Name/bandpass	Central wavelength [μm]	Width @ 50% transmission [μm]
Broad	J	1.245	0.160
	H	1.65	0.30
	K	2.215	0.41
	J+H	1.4825	0.635
	H+K	1.96	0.92
Narrow	1% @ J	1.25	1%
	1% @ H	1.65	1%
	1% @ K	2.2	1%
Shortpass	SP 2.4	50% cut-off at 2.42μm	

Note that a dichroic beamsplitter will always be in place that sends part of the light to the science detector and lets part of the light pass through to the field of the fringe tracker (see Sect. 5.15.1 and Fig. 9). If the fringe tracker detector is placed behind the beam splitter (as is typical for LINC-mode) it will not receive the same bandpass as the science detector; if it is placed outside of the area covered by the beamsplitter (typical for NIRVANA-mode), the fringe tracker can receive broadband NIR light (see Sect. 5.15.1 and Fig. 9). If desired, the available filters can then be used to match the bandpasses exploited by the science channel and the fringe tracker.[3]

[3]This will be preferred in case the identification of the central fringe turns out to be difficult. If science channel and fringe tracker do not use the same bandpass, fringe tracking on the central fringe will be important, because otherwise atmospheric fringe dispersion will lead to a loss of resolution on the science detector.

Plans are emerging to implement a non-dichroic beam splitter that would send a fraction of the broad-band light to the science detector and let the remainder pass through to the FFTS. Even though this will reduce the efficiency of the science observations by a factor TBD, it will be a useful option for early commissioning and also later on for science of bright enough objects as it makes it possible to perform fringe tracking and science observations in the same bandpass even when the guide star is on axis.

5.4 Point-spread function and modulation transfer function

At 100% Strehl ratio the LINC-NIRVANA point spread function (PSF) corresponds to the Airy pattern of a single 8.2m telescope superimposed by interference fringes created by the operation of two 8.2m telescopes in Fizeau interferometric mode. Due to the maximum optical extent of 22.6m (the line connecting the extreme points of both telescope primary mirrors which determines the highest accessible spatial frequency, see Fig. 2) approximately three fringe maxima fit into the central maximum of the 8.2m Airy distribution. This is shown in Fig. 3 (top) for a monochromatic PSF produced by four different values of the optical path difference (OPD), i.e. phase differences, between the optical paths from the two telescopes of 0, $1/3\pi$, $2/3\pi$ and π.

The center panel of Fig. 3 shows the modulation transfer function (MTF) of an ideal Fizeau interferometer at the LBT which describes the fraction of transmitted light as a function of spatial frequency. The lower panel of Fig. 3 demonstrates by way of a few examples which baselines of the binary telescope aperture form the individual lobes of the MTF (see AD10 for more details).

A comparison of the LINC-NIRVANA PSF with that of a single-dish 23m telescope can be found in AD7 (figures $15-18$ and $23-24$). The LBT produced fringes are about 30% narrower than those of a full 22.6m telescope. [4]

5.5 Pixel sampling and field-of-view

The LINC-NIRVANA science detector is a Rockwell HAWAII-2 PACE FPA (see aslo next subsection) with 2048×2048 pixels of size 18μm corresponding to 5.11mas on the sky. Hence the total field-of-view (FoV) is $10.5'' \times 10.5''$. More details on the science detector can be found in AD8.

As one can see from Table 3 that assumes that the interference fringes are aligned with the detector colums (see however Sect. 5.7) the pixel width is not sufficient for optimal sampling of the central fringe in the J-band, effectively leading to a loss in spatial resolution. Only at somewhat longer wavelengths is the sampling criterion (two pixels per FWHM) fulfilled.

Table 3: PSF sampling.

Wavelength	FWHM of central fringe [pixel]	Separation of central minima [pixel]
1.1 μm (monochromatic)	1.5 (2.0)	3.1 (4.8)
J-band	1.7	3.1
H-band	2.4	4.2
K-band	3.3	5.6

For comparison, values in brackets for the 1.1μm wavelength correspond to a full single-dish 23m telescope.

[4] $(\lambda/22.6\text{m}) \;/\; (\lambda/[2\ 14.4\text{m}]) = 28.8/22.6 = 1.3$

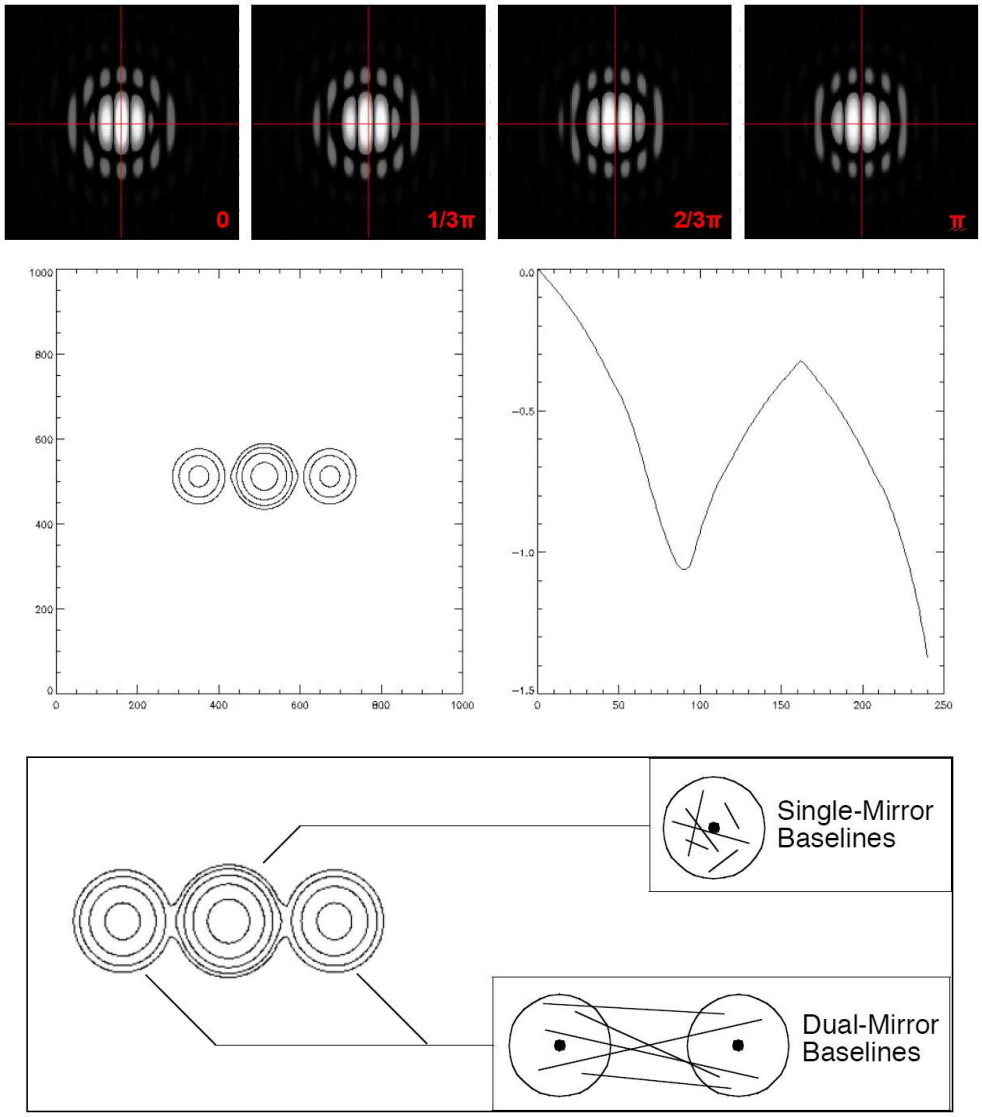

Figure 3: **Top:** Monochromatic LINC-NIRVANA PFSs for OPDs of 0, $1/3\pi$, $2/3\pi$ and π. **Center:** The instantaneous MTF of a perfect Fizeau imager on the LBT; left: 2D contour plot of the MTF (logarithmic contours); the central lobe is the 8.4 meter MTF, and the two side lobes correspond to baselines spanning the two telescopes; right: cut through the MTF, showing main and subsidiary peaks. **Bottom:** Origin of the dual lobes in the MTF of a Fizeau imager on LBT.

5.6 Science detector characteristics

The main characteristics of the science detector are summarized in Table 4. Note, however, that full testing of the science detector has not yet commenced at the time of writing this document. Therefore, the quoted values are either design values or values provided by the supplier and need to be verified. Read-out-noise values are taken from measurements of the similar HAWAII-2 detectors for LUCIFER-1 and 2. It is planned to make up to four different standard read-out modes will be available, namely:

- Double-correlated read
- Line-interlaced read
- Fowler sampling
- Sample up the ramp

The double-correlated read and the line-interlaced read are not read-out noise (RON) optimized and therefore suitable mostly for bright objects, whereas Fowler sampling and sample up the ramp make it possible to suppress RON and are therefore preferred for faint objects. A technical description of the first three modes can be found in AD9. Note, however, that the realisation of some these modes depends on yet to be determined properties of the science detector so that not all modes may become available in the end. At minimum two modes will be offered consisting of one of the two low-RON and one of the two high-RON modes.

Additionally, a "rapid-window" read-out mode is currently under development that allows to read out a smaller detector region at high frequency while at the same time integrating longer on the rest of the detector. This mode can be employed to observe a bright (value TBD) target to be placed in the window without saturation relative to faint reference sources, e.g. for precision astrometry. It will be characterized in due time. Reading a window rapidly while exposing longer on the rest of the detector is a feature offered by the latest generation of near-infrared detectors such as the HAWAII-2-RG. With the LINC-NIRVANA detector this cannot be fully achieved, but the following compromise will be implemented in order to approach this functionality. In practice not only a small window will be read out rapidly but a complete stripe of rows (or columns) in the quadrant that contains this window. Simultaneously, a similar stripe rotated by 90°, 180°, 270°, respectively, is read out rapidly in the other three quadrants. Fig. 4 provides two examples for this. If needed, one can insert the stripes of data back into the frame and recover the complete image. The area of the stripes will, however, have collected more read-out noise than the longer exposed region of the detector.

Table 4: The science detector, a Rockwell HAWAII-2 PACE FPA

General	Number of pixels	2048×2048		
	Pixel size	18μm $\equiv$ 0.511mas		
	Field of view	$10.5'' \times 10.5''$		
	Full-well capacity/saturation	$100,000$ e$^-$ $\equiv$ $65,000$ ADU		
	Linear until	$\approx 80,000$ e$^-$ $\equiv$ $52,000$ ADU		
	Conversion factor	1.5 e$^-$/ADU		
	Read-out-noise: high-RON mode	$\approx 15 - 20$ e$^-$		
	low-RON mode	≈ 5 e$^-$ [(a)]		
Quantum efficiency[(b)]	J-Band	0.64 $\pm$ 0.035 e$^-$/ph		
	H-band	0.79 $\pm$ 0.042 e$^-$/ph		
	K-band	0.76 $\pm$ 0.039 e$^-$/ph		
Timing information[(c)]	**Double-correlated read**		**Line-interlaced read**	
Minimum exposure time	0.8 s		1.6 s	
Cycle time	2.4 s		3.2 s	
Overhead	1.6 s		1.6 s	
	Fowler Sampling with			
	4 reads	**8 reads**	**16 reads**	**32 reads**
Minimum exposure time	1.6 s	3.2 s	6.4 s	12.9 s
Cycle time	3.2 s	6.4 s	12.9 s	25.8 s
Overhead	1.6 s	3.2 s	6.4 s	12.9 s
	Sample up the ramp with			
	4 reads	**8 reads**	**16 reads**	**32 reads**
Minimum exposure time	2.4 s	5.6 s	12.1 s	25.0 s
Cycle time	3.2 s	6.4 s	12.9 s	25.8 s
Overhead	0.8 s	0.8 s	0.8 s	0.8 s

Notes: (a) for ≥ 2 min of accumulated exposures
(b) Values provided by the supplier
(c) Design values to be corroborated

5.7 Field and fringe (de-)rotation

Because of the sky rotation in an alt-az-mounted telescope the science detector must constantly be derotated during an exposure in order to avoid image blurring.[5] However, this causes a changing orientation of the telescope baseline in the science image (which would otherwise remain stable). While the distribution of objects on the science detector is maintained, the PSF rotates which leads to a smearing out of the interference fringes and thus to a loss of fringe contrast and spatial resolution (see also AD10 and AD11).

To minimize the loss of fringe contrast a limit of no more than $\pm 15^\circ$ of PSF rotation with respect to the detector columns is placed. When this limit is reached, the derotator of the science detector is reset with the effect, that the original orientation of the PSF (and hence that of the fringes) is restored, but the field is now rotated with respect to the previous orientation. Note that 30° is also the maximum possible rotation range for the science detector unit. Therefore, there is no flexibility

[5] Likewise derotation mechanisms exist for all wavefront sensors, and the fringe tracker will follow a predetermined trajectory in order to follow a star.

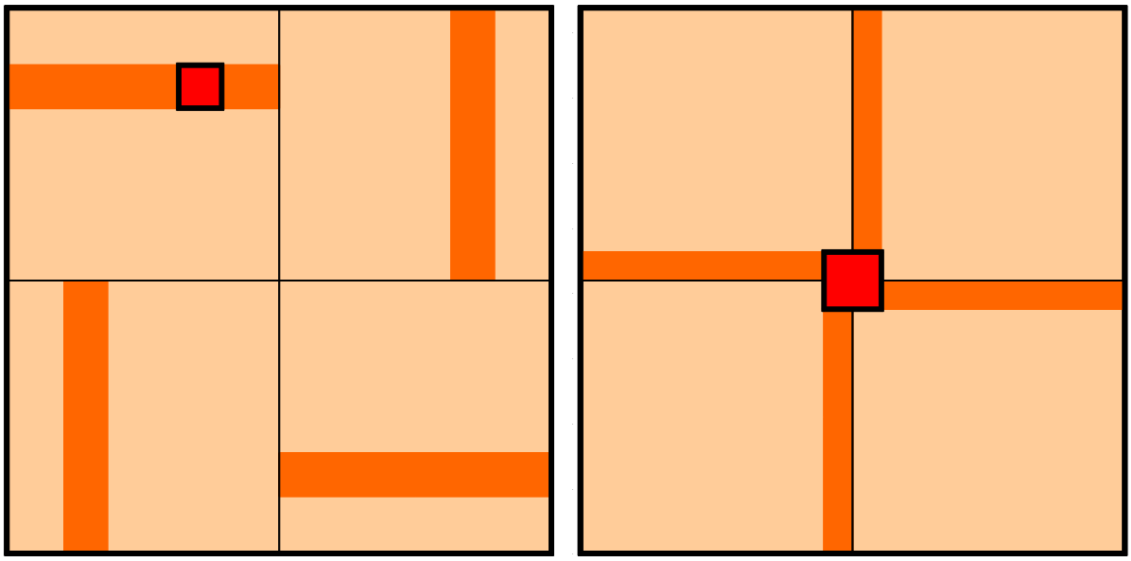

Figure 4: Examples of the science detector feature relevant to the rapid-window read-out mode. In order to avoid saturation by a bright object one would like to place this object in a small window (such as the red square) that is read out rapidly while the rest of the detector is used to expose longer. In practice, however, a complete stripe must be read out rapidly in each quadrant (shown in orange). Left: desired window off-center. Right: desired window at center.

in the choice of the orientation of the detector on the sky unless the total amount of PSF rotation is reduced further.

The rate of field rotation as a function of sky coordinates can be extracted from Fig. 5 that shows how the parallactic angle (i.e. the position angle of the zenith direction at a certain sky position) changes with hour angle and declination.[6]. Only hour angles after meridian passage of the sky position are plotted. To determine the parallactic angles before meridian one has to correspondingly prolong the solid lines to the left of the plot such that they are rotationally symmetric around either the 180° or the 0° position angle (for declinations greater or less than the geographic latitude, respectively). Note that in the plot lines end when the sky region sets below the horizon (right ends of the lines).[7]

Close to zenith field rotation becomes rapid so that only short exposures are possible before the rotation angle exceeds 30°. This is shown in Fig. 6 where the maximum exposure time as a function of hour angle and declination is given.

[6]The parallactic angle is defined as the angle between the great circle through a celestial object and the zenith, and the hour circle of the object

[7]The plot has been made for Kitt Peak Observatory, but is very close to the correct plot for Mt. Graham because the geographic latitude of both sites is almost identical. Geographic coordinates of Kitt Peak: W 111°35.8′, N +31°57.5′.

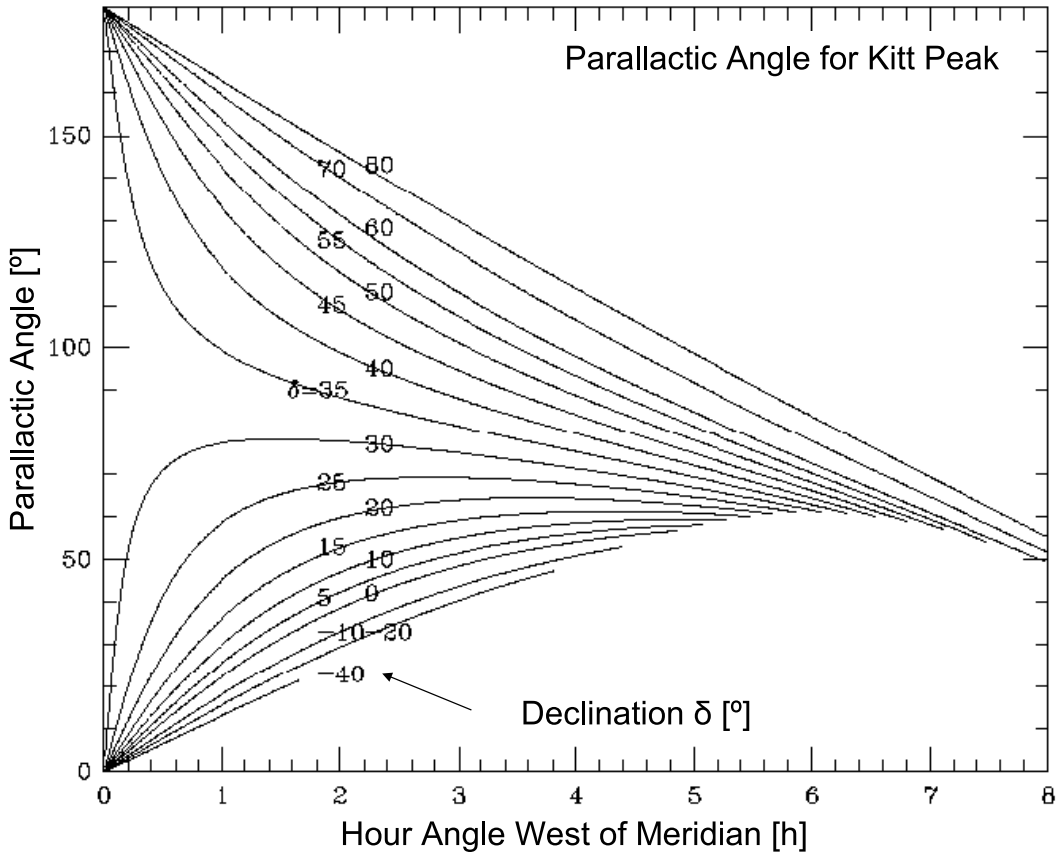

Figure 5: Parallactic angle as a function of hour angle after/west of meridian) and declination δ (labels of the curves). The corresponding parallactic angles before/east of the meridian are negative (modulo 360°).

5.8 How fringe rotation provides a 23m telescope

Exploiting the rotation of the fringes is one of the main observational techniques for attaining the full resolution of a 23m telescope with LINC-NIRVANA. For this purpose the same science field is observed at various orientations of the interference fringes so that the high resolution is obtained in different directions. An ideal case for image reconstruction would be, say, three fringe orientations at 0°, 60°, and 120° parallactic angle, respectively. As can be seen from Fig. 5 this cannot be achieved in all regions of the sky. For astrometric measurements of point sources two parallactic angles should be sufficient, ideally separated by 90°.

The LINC-NIRVANA data reduction software (LDRS) under development at MPIfR Bonn, Germany (as well as the Airy-LN package developed by the University of Genova, Italy) will provide image reconstruction tools to convert these images into a combined high-resolution image (e.g. via Richardson-Lucy deconvolution, Building Block methods that can accommodate space-variant PSFs, etc.). Note, however, that because one will typically attempt to keep the fringes parallel to the detector columns (otherwise a slight resolution loss will occur) during the different visits to the same sky region the field will have different orientations so that the edges of the detector are lost for

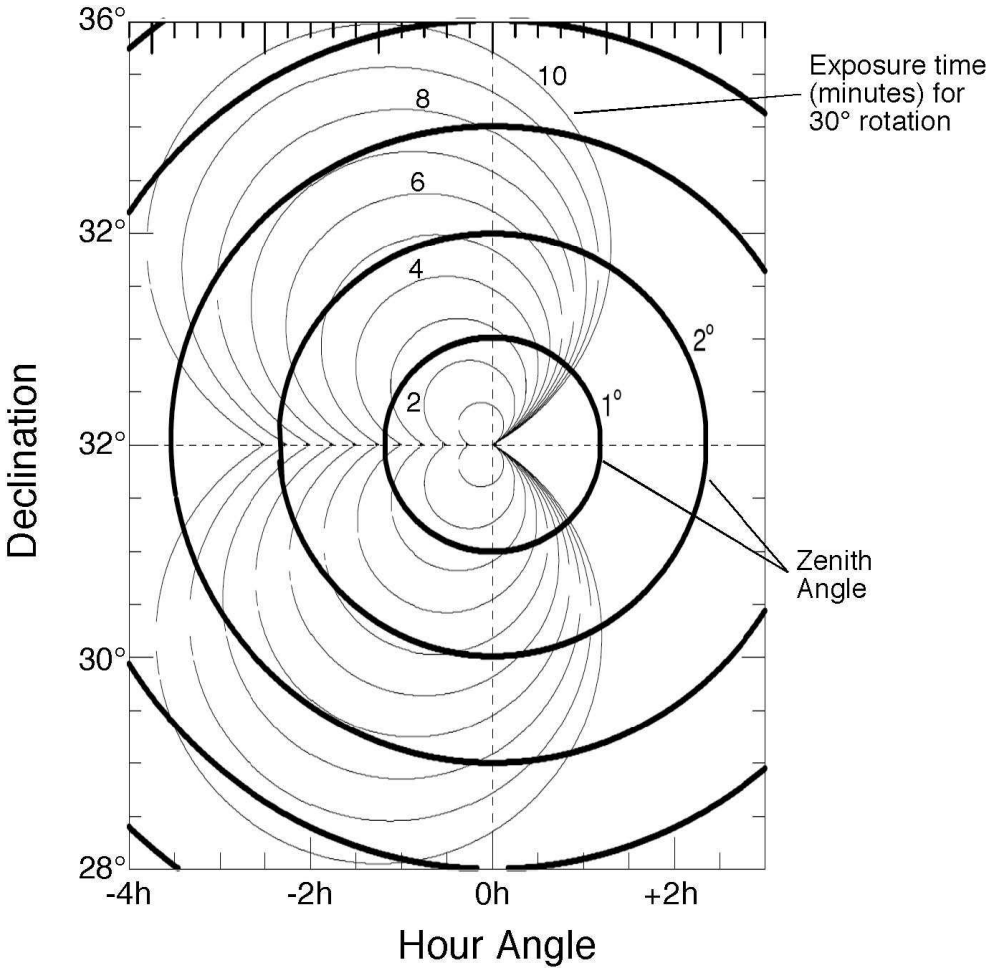

Figure 6: Exposure time for 30° sky rotation as a function of hour angle and declination. The heavy contours show the angular distance from zenith, while the thin contours give the exposure time during which the sky rotates by 30°. Exposure times longer than 10 min are not considered (cf. Sect. 5.11). The asymmetric distribution of the thin contours results from the fact that the coordinates correspond to sky positions at the beginning and not at the middle of the exposure.

the combined image (cf. Sect. 5.7). Planning tools to select the possible parallactic angles will be provided to the users as part of the LINC-NIRVANA observation preparation software (LOPS).

5.9 Minimum and maximum zenith distance

At zenith field rotation becomes too fast for the telescope dome to follow. Therefore, a minimum zenith distance of 1.5° must be observed.

Even though the telescope can point to lower elevations it is not foreseen to routinely use the instrument at zenith distances greater than 60°, because of excessive mechanical flexure effects (see next subsection). In fact, many of the performance specifications for the instrument were made only for zenith distances up to 60°.

5.10 Mechanical flexure effects

The instrument team will devote a substantial amount of effort into the characterisation and compensation of mechanical flexure occuring when the instrument is tilted along with the telescope. The amount of flexure will typically increase with the tilt angle. Therefore, it is conceivable that low-elevation observations will be difficult in the early implementation phase.

5.11 Maximum exposure time

LINC-NIRVANA will support a maximum exposure time of 10 min. This performance specification has been established, because for longer exposures the stable functioning of the various control loops of the instrument cannot be guaranteed, because of residual effects from flexure, alignment imperfections, and thermal effects (among others). The requirement to obtain 10 min of stable performance was chosen, because under typical conditions an exposure reaches the background limit in K-band after 10 min even in a narrow band filter.

Note, however, that the need to reset the derotator of the science detector limits this maximum exposure time further in sky regions close to zenith (see Fig. 6 and Sect. 5.7).

5.12 Required ambient temperature range

LINC-NIRVANA is specified to be operational within the ambient temperature range from −10°C to +25°C.[8] Note, however, that full characterization of the complete instrument below +15°C will probably be difficult to achieve in the labs at MPIA Heidelberg. Therefore, full performance at lower temperatures cannot be expected at the beginning of operations.

Table 5: Limiting magnitudes at airmass = 1.0

	J-band @1.25μm					H-band @1.65μm					K′-band @2.12μm @$T_{\rm ambient}$ = +5°C				
Strehl	0.2	0.4	0.6	0.8	1.0	0.2	0.4	0.6	0.8	1.0	0.2	0.4	0.6	0.8	1.0
$T_{\rm exp}$															
10 min	24.5	25.3	25.7	26.0	26.2	23.3	24.0	24.5	24.8	25.3	22.4	23.1	23.6	23.9	24.1
30 min	25.2	25.9	26.4	26.7	26.9	23.9	24.7	25.1	25.4	25.6	23.0	23.8	24.2	24.5	24.8
60 min	25.6	26.3	26.8	27.1	27.3	24.3	25.0	25.5	25.8	26.0	23.4	24.1	24.6	24.9	25.1

5.13 Limiting magnitudes

Limiting magnitudes at airmass = 1.0 for a point source signal-to-noise ratio of five (SNR = 5) as integrated over the central peak of the Airy disk are given in Table 5 for different exposure times and Strehl ratios. Listed are the limiting magnitudes for the J-band and the H-band, as well as for observations in the K′-band at an ambient temperature of $T_{\rm ambient}$ = +5°C. The approximation was made that the fraction of source flux in the central peak of the Airy-disk is equal to the Strehl ratio and independent from the fringe contrast. Since there is a substantial amount of thermal background

[8] In earlier documents a range from −15°C to +25°C can be found, but the low-temperature limit has been relaxed more recently.

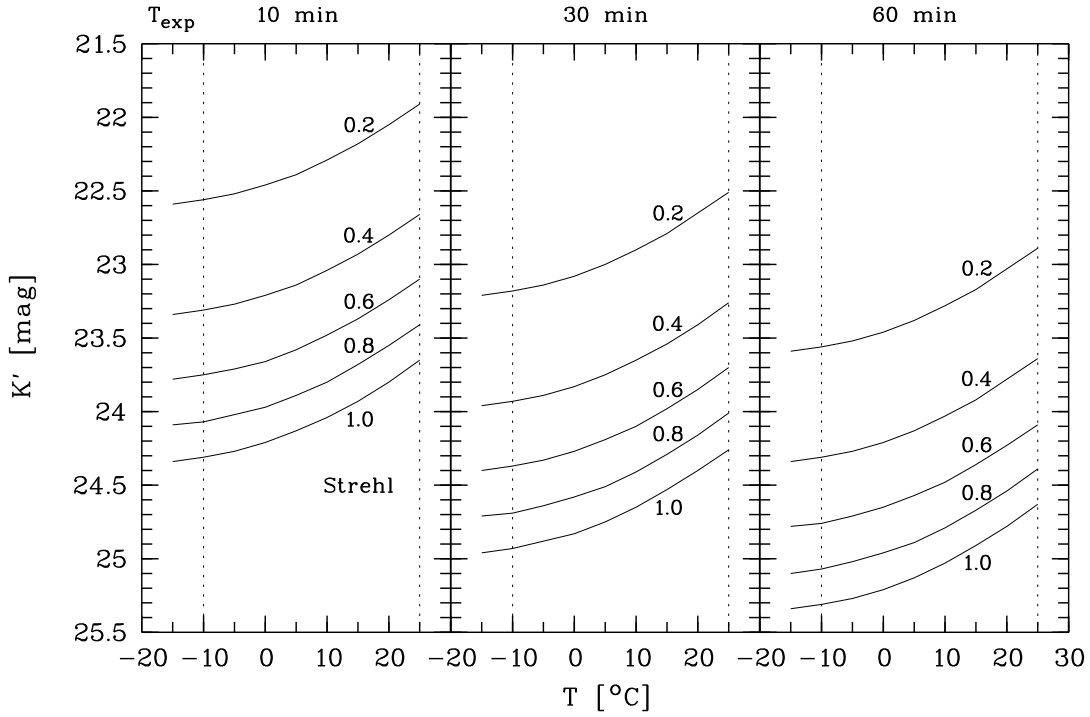

Figure 7: Limiting magnitudes at arimass = 1.0 in K′ for an SNR = 5 integrated over the central peak of the 8.2m Airy disk of a point source as a function of ambient temperature. The three panels of the plot correspond to different values of the total exposure time of 10 min, 30 min, and 60 min (from left to right) while the different curves within each panel correspond to different values of the Strehl ratio of 0.2, 0.4, 0.6, 0.8, and 1.0 as labelled. Vertical dashed lines delimit the temperature range specified for LINC-NIRVANA science operations.

in the K-band Fig. 7 shows the limiting magnitudes for K′ als a function of ambient temperature and assuming the same values of the other parameters.[9]

5.14 Saturation limits as a function of exposure time and filter

In order to avoid detector saturation single exposure times must be kept short for bright objects. With 0.8 s the shortest exposure time can be achieved in the double-correlated read-mode (see Table 4 and Sect. 5.6) that is appropriate for bright targets. The point source magnitudes at which the detector saturates or reaches the non-linear regime at this minimum exposure time are given in Table 6 as a function of Strehl ratio and science filter and assuming airmass = 1.0 and fringe contrast = 1.0.

Brighter objects can be observed with narrow-band filters; e.g. a filter with 1/20 of the throughput of a broad-band filter will cause saturation to occur only for stars that are 3.25 mag brighter.

[9]If the 60 min exposure time corresponding to the right panel in Fig. 7 were employed in a single exposure, the dominant high background alone would reach the non-linear detector regime (estimated to begin at 80,000 e^-; see Table 4) when temperatures exceed 20°C and the saturation limit (beyond 100,000 e^-) when temperatures exceed 24°C. However, single exposures longer than 10 min will not be offered; see sect. 5.11.

Table 6: Saturation magnitudes for the minimum exposure time of 0.8 s, airmass = 1.0 and fringe contrast = 1.0.

	Saturation			Non-linearity		
Strehl	J	H	K′	J	H	K′
0.2	9.8	8.8	7.8	10.1	9.0	8.0
0.4	10.6	9.5	8.5	10.8	9.8	8.8
0.6	11.0	10.0	9.0	11.3	10.2	9.2
0.8	11.3	10.3	9.3	11.6	10.5	9.5
1.0	11.6	10.5	9.5	11.8	10.8	9.8

Note that this section will need to be updated in order to reflect the true LINC-NIRVANA filters (e.g. the J-band is already subdivided into two bandpasses; see Table 1 in Sect. 5.3.1). Saturation magnitudes for the FFTS star will be provided when the details of the FFTS are better defined. The same holds for the wavefront sensing stars.

Table 7: Fields and guide stars.

Sensor or detector	**Field type**	**Field diameter**	**Reference stars**			
			Nr. of stars		**Integrated magnitude**$^{(a)}$	
			LINC mode	**NIRVANA mode**	**LINC mode**	**NIRVANA mode**
GWS sensor	annular	$2.88' - 6'^{(b)}$	0	≤ 12	n.a.	$R = 13 - 15$
MHWS sensor	circular	$2'$	1	≤ 8	$R \leq 16$	$R \leq 16$
FFTS sensor	oval	$1' \times 1.5'^{(c)}$	1	1	$K \leq 12 - 13$	$K \leq 13 - 14$
Patrol camera	circular	$2'$	MHWS field			
FFTS detector	square	$\leq 2.5'' \times 2.5''^{(d)}$	FFTS star			
Science detector	square	$10.5'' \times 10.5''$	n.a.			

(a) All values are indicative only and need to be verified. Minimum and maximum values refer to the early and late instrument implementation phases, respectively (see Sect. 4.3).

(b) Inner and outer diameters of the unvignetted region; used only in NIRVANA mode. Vignetting occurs within the also accessible annulus between diameters of $2'$ and $2.88'$ and some at $6'$ on the tertiary (TBC).

(c) See Fig. 9 for vignetting.

(d) Value depends on chosen size of detector window. The maximum value given here is for one quadrant and only used for setup. In closed-loop fringe tracking a typical values is 160×80 mas.

5.15 Guide stars

The performance of LINC-NIRVANA will depend strongly on the availability of suitable guide stars. Fig. 8 shows a comparison of the usable sky areas for the different sensor systems of the instrument. The sky areas are also summarized in Table 7 and compared with the FoV of the science detector (cf. Sect. 5.5), the FoV of the FFTS detector,[10] and the FoV of the Patrol Camera (which is identical to the FoV of the MHWS). The FFTS detector as well as the individual guide star acquisition systems

[10]Of the FFTS detector mostly a small window of typically 32×16 pixel corresponding to 160×80 mas will be read out for fringe tracking. A larger window on the same detector will be used to track flexure via a dedicated optics system called the "periscope."

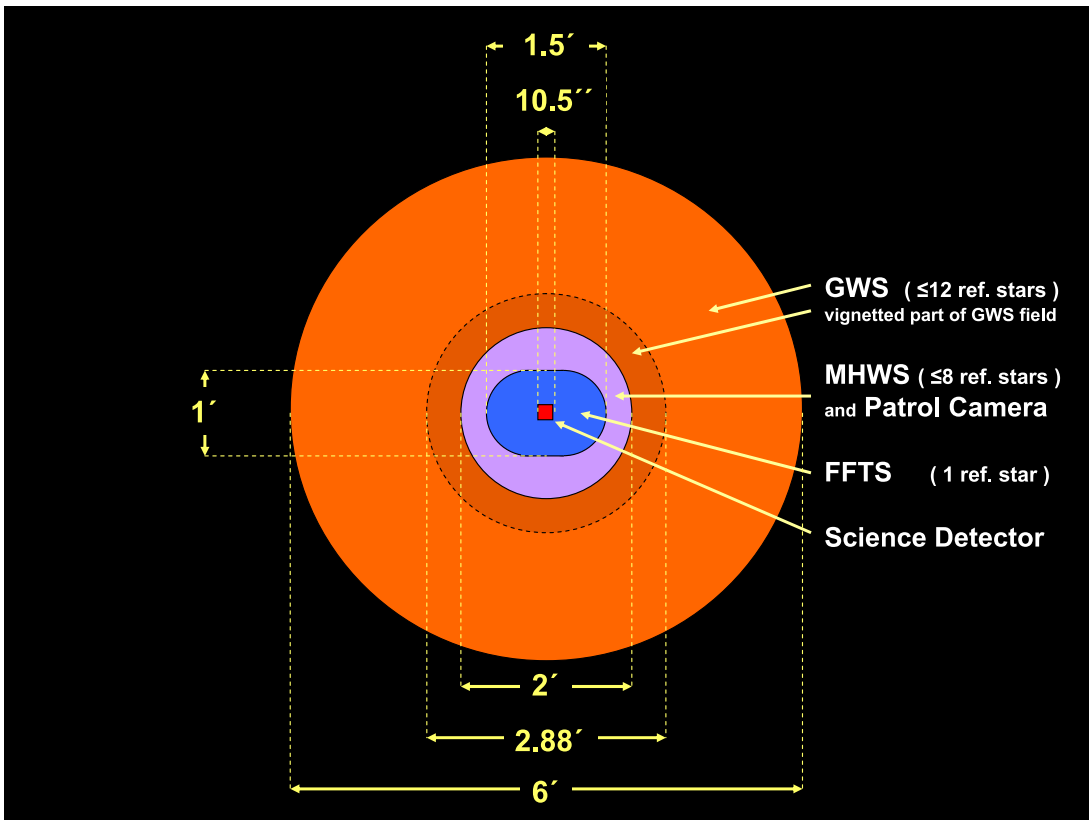

Figure 8: Comparison of the various accessible fields and fields of view of LINC-NIRVANA. While the GWS field is the annular region shown in orange (see also Table 5) the fields of all the other systems overlap as they are either circular, oval, or square and contain the central viewing direction.

of the GWS and the MHWS (the so-called "star enlargers" that hold the pyramids used in this type of wavefront sensor along with their relay optics) can be moved on the sky in order to find suitable reference stars as described in Sects. 5.15.1 to 5.15.3.

Also indicated in Table 7 is the maximum number of guide stars per sensor and observing mode (LINC mode or NIRVANA mode) as well as the estimated requirement for the (integrated) magnitudes[11] of the reference star(s), expressed as magnitude ranges from whose endpoints the respective requirement for the early and late implementation phases of the instrument can be taken.

5.15.1 FFTS guide star

The FFTS detector can be moved within an oval field with diameters of $1' \times 1.5'$ (perpendicular and parallel to the binary telescope baseline, respectively) in order to find a reference star for fringe tracking. This field is depicted in Fig. 9 (blue area). A dichroic beamsplitter must be inserted into the beam in order to send light both to the science detector and the near-on-axis area of the FFTS field. As shown by the black areas in Fig. 9 the mount of this dichroic causes vignetting in an ring around field center as well as along the shadows of the two bars that connect the dichroic holder with the dichroic wheel.

[11]The integrated magnitude corresponds to the summed brightness of all reference stars used by the sensor. It can be obtained by converting the individual magnitudes of all stars into fluxes, co-adding them, and expressing the sum again in magnitudes.

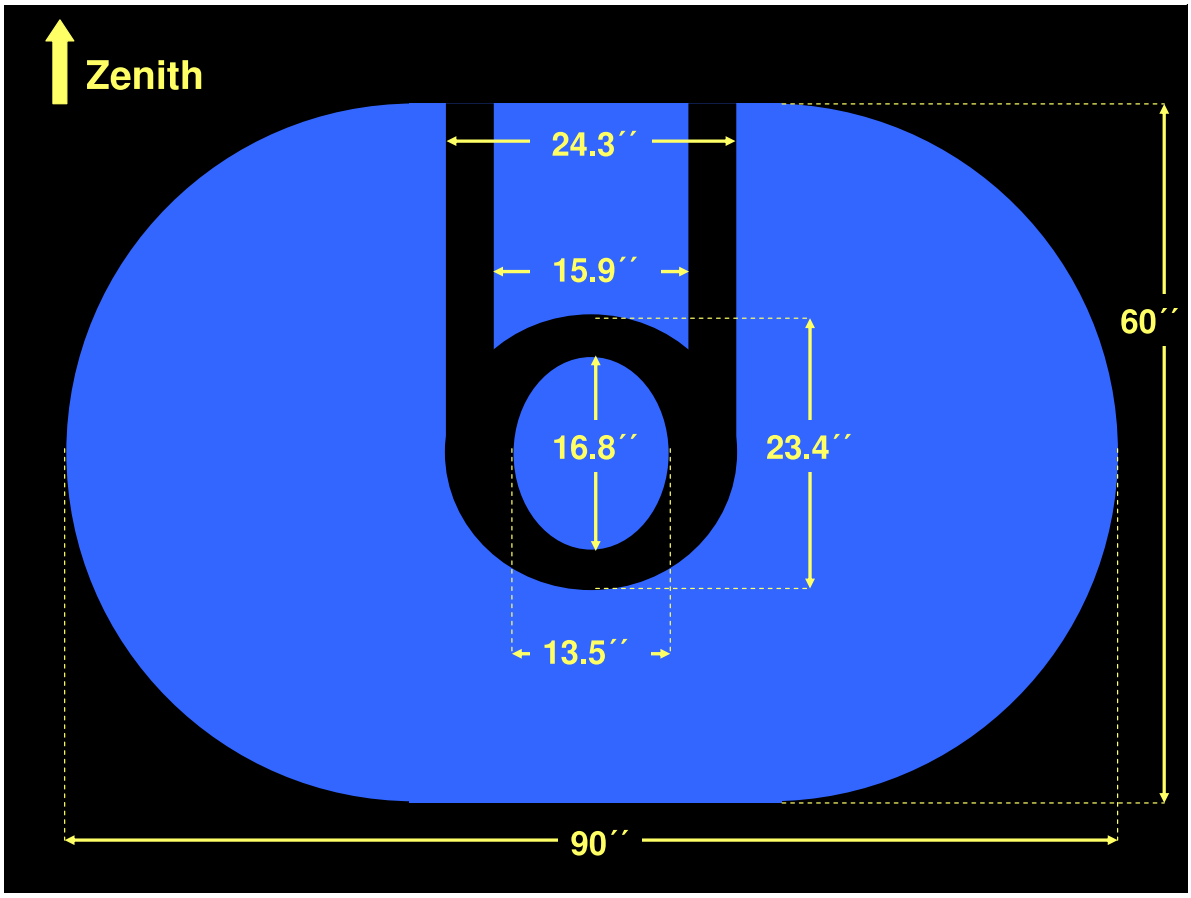

Figure 9: Outline of the field in which the FFTS can search for a guide star (blue area). Black areas inside the blue field delimit the shadow of the cold dichroic mount where vignetting occurs.

When placed off-axis the FFTS reference star will have to be moved in the field along circular trajectories around the field center in order to track field rotation. During this operation the vignetted regions must be avoided. Likewise, it will not always be possible to fully use regions further away than 30″ from the optical axis because the tracking trajectory will eventually place a reference star outside of the field. Going off-axis with the fringe tracker will be a frequent case in NIRVANA-mode, whereas the LINC-mode requires guide stars that are basically on-axis or placed just a few arcsec away from the optical axis which is, e.g., necessary for dithering (see Sect. 5.17). Such stars will in most cases need to be located inside the central unvignetted elliptical field.

Fringe/flexure tracking and science observations will often be performed in different bandpasses: For a near-on-axis guide star also the light reaching the FFTS will pass through the dichroic with the effect that fringe/flexure tracking and science observations will use different parts of the spectrum; when a guide star is placed outside of the area covered by the dichroic, fringe-flexure tracking can select standard bandpasses with its own filters (Table 2) out of the broad-band NIR light it receives. This may or may not be similar to the bandpass used for the science observations (cf. Sect. 5.3.2).

As already noted in Sect. 5.3.2, plans are emerging to implement a non-dichroic beam splitter that would send a fraction of the broad-band light to the science detector and let the remainder pass through to the FFTS. Due to the resulting loss of effeiciency this mode would mostly be used for ealy commissioning and pn bright targets.

The LINC-NIRVANA observation preparation software will make it possible to consider the exact geometry and constraints of the fringe tracker field.

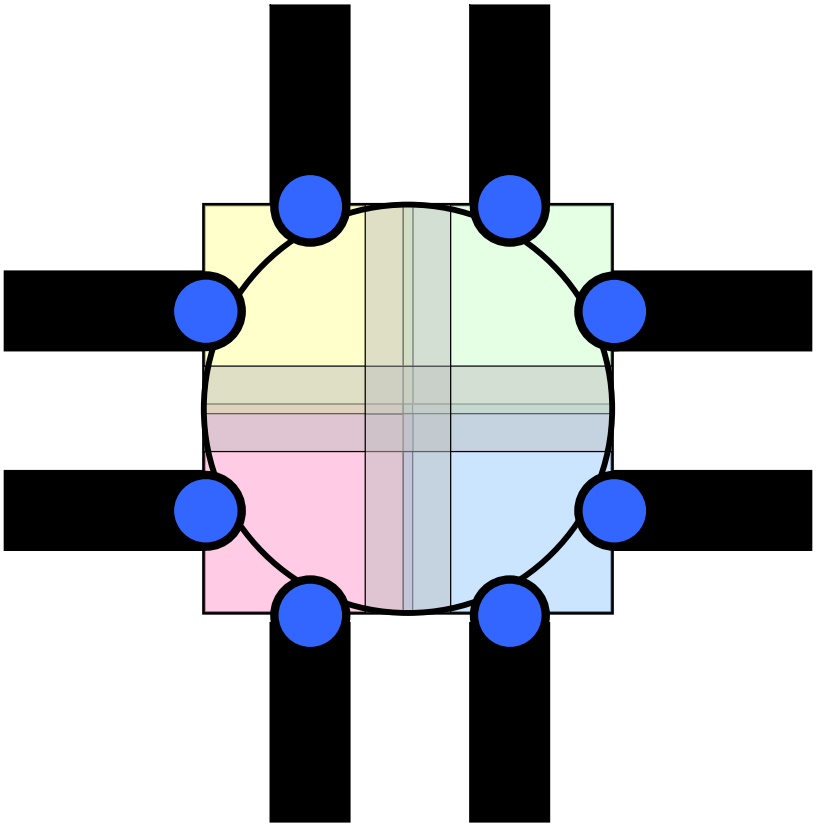

Figure 10: Schematics of the MHWS layout. Within a field of 2′ diameter (large circle) up to eight star acquisition systems ("star enlargers") can be placed shown here as blue circles at the end of their positioning arms. The centers of the blue circles are occupied by the wavefront sensor pyramids. All star enlargers are shown here in their park position. For restrictions on the placement of the star enlargers see the text.

5.15.2 AO stars LINC-mode

In LINC-mode which uses a single natural guide star for the AO correction one of the eight pyramid systems ("star enlargers") of the MHWS will be used. For this purpose the pyramid is placed at (or near) the center of the sensor field (see Fig. 10). Since the light that the MHWS receives passes through a dichroic beamsplitter that sends the NIR part of the light to the science channel, only visible light with wavelengths in the range $0.6 - 0.9$ μm reaches the MHWS (see AD12) so that wavefront sensing is performed in a bandpass that roughly resembles the combined R and I-bands (with the larger contribution to the total flux coming from the R-band).[12] The GWS is not used at all in LINC-mode.

[12]The exact spectral range that will be exploited depends on the transmission properties of all optics involved and on the quantum efficiency as a function of wavelength of the E2V CCD 39 detector of the MHWS.

5.15.3 AO stars NIRVANA-mode

MHWS:

In NIRVANA-mode up to eight natural guide stars can be acquired by the MHWS. Again, wavefront sensing is performed in the $0.6 - 0.9$ μm bandpass. The MHWS will be conjugated to a height of 7.1 km above the telescope. At zenith, this corresponds to an atmospheric layer of the same altitude, and at higher airmass it corresponds to a correspondingly lower layer given. The altitude a of this layer is given by

$$a = 7.1 \text{ km} \times \cos z$$

where z is the zenith distance angle.

Fig. 10 shows the layout of the MHWS star enlarger system. A FoV of $2.0'$ diameter is accessible (large circle). The large square with a side length of also $2.0'$ delimits the mechanical travel ranges of the star enlargers. Of the eight star enlargers pairs two share the same quadrant with a side length of $60.6''$. There is a small overlap of $1.2''$ between the quadrants with the effect that each star enlarger can be placed into a small strip within both of its neighbouring quadrants and in principle all star enlargers can reach the field center.

Due to limited travel ranges of the MHWS star enlargers not more than two star enlargers can be positioned per quadrant with the exception of the small overlap regions. Star enlargers collide with each other when they reach a minimum separation equal to their diameter.[13] Therefore, each pair of guide stars must have a minimum separation of $23''$. Note that collisions must not only be avoided between the two star enlargers of the same quadrant, but also within a cross-shaped area centered on the field center (semi-transparent grey shaded area in Fig. 10) where collisions between star enlargers from neighbouring quadrants are possible. The width of each of the bars of the cross is $24''$.

GWS:

Up to 12 natural guide stars can be acquired by the GWS. It is conjugated to the atmospheric ground-layer, or more precisely, to a height of 100 m above the telescope. Even though both infrared and visual light reaches the GWS, wavefront sensing is done in the visual mostly for reasons of the response of the CCD-detector of the GWS.[14]

Fig. 11 shows the schematics of the GWS star enlarger system. 12 stars can be positioned within symmetrically placed regions (semi-transparent coloured squares) covering the $6'$ diameter FoV (large circle). Concerning collisions between the star enlargers similar restrictions as for the MHWS apply, however, accordingly adapted to the modified geometry. Note that there is considerable overlap between the travel ranges of the individual star enlargers. Also note that the inner circular region of $2.88'$ does not belong to the usable FoV (see Table 7 and Fig. 8).

5.16 Expected Strehl ratios

5.16.1 On-axis Strehl LINC-mode

In LINC-mode that exploits "classical" on-axis AO correction the highest Strehl ratios of up to 80% in H and K-band can be expected albeit only close to the optical axis. The AO correction degrades with increasing angular separation of the science field from the AO guide star roughly like a Gaussian

[13] Such collisions are, of course, excluded by both software and hardware

[14] The exact spectral range that will be exploited depends on the transmission properties of all optics involved and on the quantum efficiency as a function of wavelength of the E2V CCD 50 detector of the GWS.

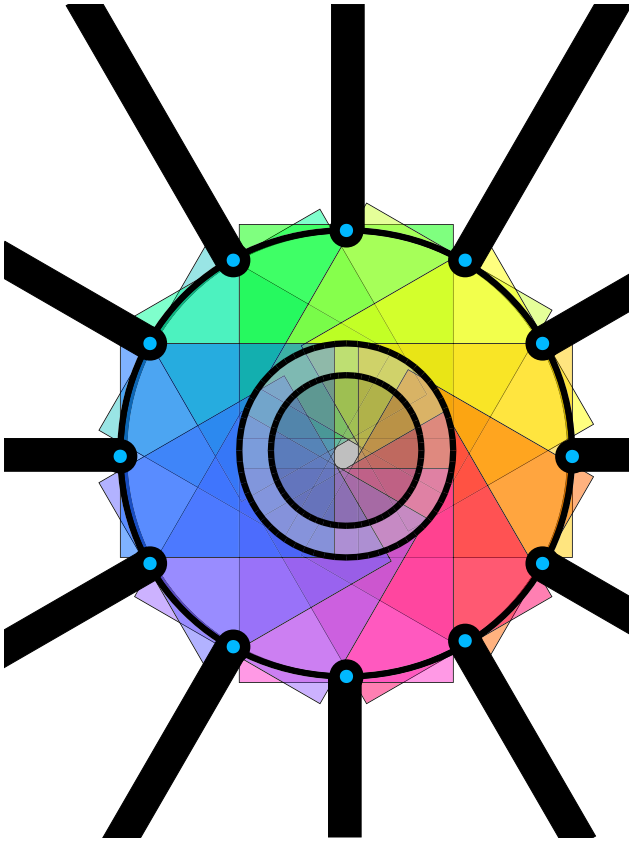

Figure 11: Schematics of the GWS layout. Within a field of $6'$ diameter (large circle) up to 12 star acquisition systems ("star enlargers") can be placed. They are shown here at their park position. Each of them can be positioned within a square area of size $2.9' \times 2.9'$. The areas accessible to the individual star enlargers have considerable overlap (visualized here by a range of semi-transparent colours). Note that the central circular region of $2'$ diameter (innermost circle) is missing from the FoV and that vignetting occurs within the annular region between $2'$ and $2.88'$ (up to the thin circle). For restrictions on the placement of the star enlargers see text.

function. It is characterized by the iso-planatic angle, i.e. the angle at which the ratio of the Strehls achieved at the sky position of interest (the science field) and for the AO guide star drops to $1/e$. The typical angular radius of the iso-planatic patch of the atmosphere above Mt. Graham is estimated to be $\approx 30''$ in K-band.[15]

Fig. 12 taken from Esposito et al. (2010; AD14) illustrates the H-band Strehl ratio achieved for different seeing values with the LBT adaptive optics secondary mirror (AOS) during its commissioning. These data were obtained with the near-infrared test camera and a pyramid wavefront sensor that employed a bandpass of $0.6 - 0.95$ μm similar to that to be used by the LINC-NIRVANA MHWS in LINC-mode. They serve as a good reference point for the Strehl ratios that will be achievable in this instrument mode.

[15] At the visible wavelength $\lambda = 500$nm Egner (2006; AD13) has determined the median iso-planatic angle for Mt. Graham to be $2.71'' \pm 1.11''$ which is 30% better than the value obtained for the Chilean sites La Silla, Cerro Tololo, and Cerro Pachon, more than 40% better than Mauna Kea (Hawaii), and about twice a large as La Palma (Canary Islands).

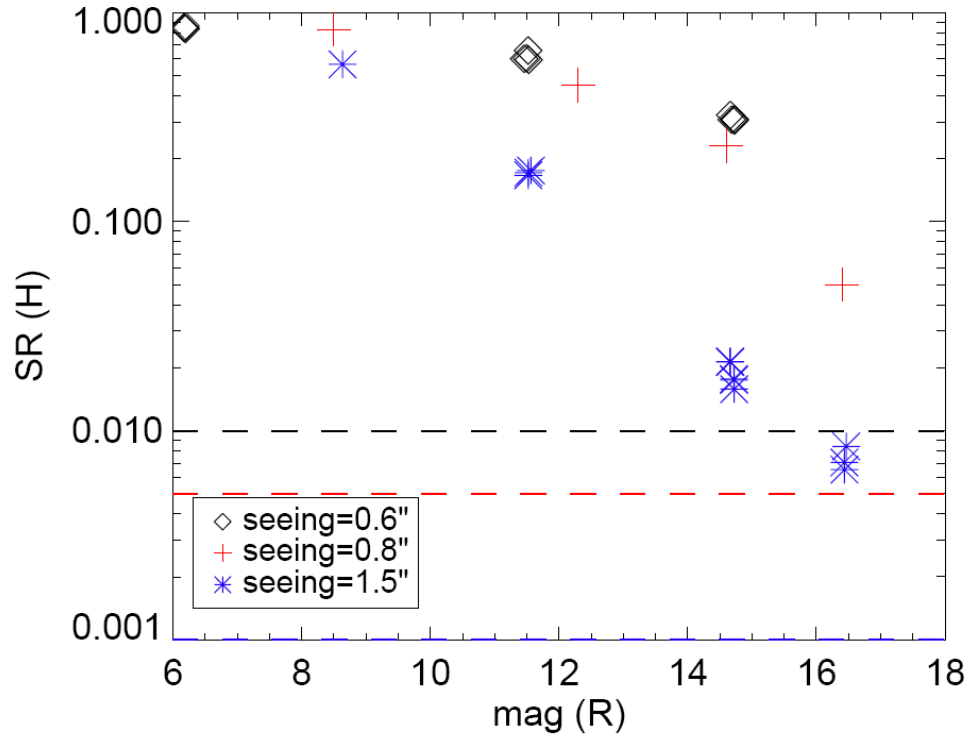

Figure 12: H-band Strehl ratios achieved with the LBT AOS (from Esposito et al. 2010; AD14): Measured Strehl ratio versus R-band magnitude for different seeing values of 0.6″, 0.8″, and 1.5″).

5.16.2 Field Strehl NIRVANA-mode

In NIRVANA-mode the AO correction will be not as good as in "classical" AO (i.e. in LINC-mode on-axis), but it will be more uniform across the FoV. Neither for the AO correction nor for fringe/flexure tracking will it be required to have a guide star on-axis so that more of the sky can be accessed (increase sky coverage). The Strehl ratios to be expected for the NIRVANA-mode can be inferred from data obtained with the MAD instrument (MAD stands for multi-conjugated adaptive optics demonstrator) that was used at the Very Large Telescope (VLT) of the European Southern Observatory (ESO).[16]

The achieved Strehl ratio with MAD in the layer-oriented MCAO mode can be taken from Arcidiacono et al. (2008; AD15) and is summarized in Table 8. The data reported in that paper for this mode were, unfortunately, obtained under relatively poor seeing conditions of 1.39″ as measured with the DIMM (differential image motion monitor) in V-band.

The expected value of the Strehl ratio in NIRVANA-mode with bright reference stars (see Table 7) is $30-40\%$ in K-band. Simulations relevant for the expected performance of the MCAO system can be found in AD16.

[16]This instrument was basically a prototype of the LINC-NIRVANA MHWS with some modifications that are not of interest here. MAD was used in two different modes: star-oriented MCAO and layer-oriented MCAO. Only data from the latter mode are relevant here, as LINC-NIRVANA will be driven in the same mode.

Table 8: MCAO performance achieved with MAD in layer-oriented mode.

Three guide stars with M_V [mag]	FWHM [″]	EE[(a)] @ 0.1″	Strehl(Br-γ) [%]	DIMM-seeing (V-band) [″]
11.059, 11.157, 12.072	0.12 ± 0.04	23.3 ± 3.9	17.3 ± 9.1	1.39″

(a) Encircled energy within a radius of 0.1″.

5.17 Dithering and nodding

During the observation of a science target the telescope pointing can be changed in small steps. Two types of movements are distinguished: those that displace the pointing direction such that an on-axis star remains within the FoV of the science detector and those for which the star is moved outside. For movements parallel to the detector axes this distinguishes movements by $\leq 5.25''$ which we call "dithering" from larger movements called "nodding". Usually, during dithering a predefined pattern of positional offsets will be followed with each step corresponding to an offset of a few arcsec. This observational strategy is mostly employed to be able to treat detector defects in the data reduction. The larger nodding movements will typically be used to alternate between a science target and a nearby field for sky subtraction.

It is also likely that different overheads are associated with small and larger offset movements because of the need to move all guide stars (FFTS, MHWS and GWS) in a combined fashion with the telescope (so-called "combined offset") or to re-acquire them. Re-acquisition will become necessary when either the precision of the combined offset is not sufficient for larger movements or the guide stars reach some mechanical limit or FoV-related limit and a larger reconfiguration of the sensor systems becomes necessary.[17]

At this point of instrument development it is not clear whether the $\leq 5.25''$ threshold defined above to distinguish dithering from nodding will also correspond to regimes with different overheads. In other words it is not clear whether dithering can always be made with combined offsets of telescope and guide stars and whether nodding will require a full re-acquisition. It is not yet known at which distance the true threshold will be. However, to illustrate the principle it is assumed in the following that the thresholds between dithering and nodding on the one hand and between combined offsets and reacquisition of guide stars on the other hand are identical.

Overheads for dithering and nodding need to be determined, but for the case that the telescope movement places the main limitation the current best estimates are the following values:

- $<$ 14 s maximum and 6 s on average per dithering step and
- 60 s maximum and 20 s on average per individual nod.

5.17.1 Overheads

Table 9 summarizes the expected overheads due to telescope preset and active optics as well as due to the acquisition of the guide stars by the sensors of the instrument and the closing of the control loops. Note that all values for the different systems of the instrument are goal values that have large uncertainties. More reliable predictions will only be possible after completion of the respective system tests in the lab or on sky.

[17] One should, of course, try to avoid being restricted by mechanical or FoV-related limits as much as possible with the help of the planning tools provided by the Observation preparation Software.

Table 9: Overhead estimates (to be verified).

	Setup/preset (parallel)	Close/adjust loops (sequentially)	Sum
Telescope (incl. active optics)	552 s (max.) 162 s (avg.)		
MHWS	60 s	60 s	
GWS	60 s	180 s	
FFTS	300 s	60 s	
LINC-mode: Effective overhead	552 s (max.) 300 s (avg.)	120 s	672 s (max.) 420 s (avg.)
NIRVANA-mode: Effective overhead	552 s (max.) 300 s (avg.)	300 s	852 s (max.) 600 s (avg.)

5.18 Interferometric performance

5.18.1 Fringe contrast

See AD17.

6 Calibration of science data

A detailed calibration plan for LINC-NIRVANA must be developed in order to define those calibrations that need to be routinely performed by the instrument operations team in order to calibrate the scientific data as well as to monitor several selected performance characteristics of the instrument.

The stability of certain instrument characteristics (flatfield and detector response, bad pixel map, dark current, read-out-noise, linearity) will have to be determined and monitored in order to decide for which applications master calibrations (such as flatfields and dark exposures) are sufficient and when dedicated calibrations must accompany science exposures.

The input of the instrument science team for the development of the calibration plan will be important.

The two fundamental calibration strategies will be on-sky calibration and calibrations using the calibration unit of the instrument.

6.1 On-sky calibration

On-sky calibration can be used for sky flatfields by observing an “empty field” during dawn or dusk in those filters that are used in the night.

6.2 The calibration unit

The calibration unit provides flatfielding via its internal light source. It also provides a range of options for alignment and testing that are more of interest for the engineer than the astronomer.

7 Data reduction

7.1 On-line quick reduction

The LINC-NIRVANA data reduction software will provide quick-look tools for data display and quick reduction. Again, the input of the instrument science team will be important in order to establish clear requirements for this.

7.2 Off-line reduction

Off-line data reduction will be possible using the data reduction software which will provide standard reduction recipes as well as a variety of image reconstruction tools emplying inversion techniques such as Richardson-Lucy deconvolution (also called the Expectation Maximization Algorithm) and the Building Block Algorithm that can handle space-variant PSFs. A future version of this document will provide more information on this.

8 Observation preparation

The LINC-NIRVANA observation preparation software provides the user with a variety of tools for the planning and optimization of the observing program. A future version of this document will provide more information on this, but see AD18.

It will be important for the development of the observation preparation software to receive feedback from the instrument science team.

Two standalone tools can already be obtained from the LINC-NIRVANA team:

1. An exposure time calculator (ETC) that allows to calculate for a point source of selectable brightness, Strehl ratio, fringe contrast, bandpass (filter) either the achieved S/N ratio as a function of exposure time or the required exposure time as a function of desired S/N ratio. Detector non-linearity and saturation are taken into account and a plotting utility is included. This tool is a java-based graphical user interface (GUI). It will also be part of the overall observation preparation software.
2. An IDL-based point-spread-function simulator (PSF simulator) for detailed simulations of LINC-mode PSF's.